2-26-2019

A Practical, Quantitative Electrostatics Experiment

Bryan K. Armentrout
Nova Southeastern University, ba387@nova.edu

Diego Castano
Nova Southeastern University, castanod@nova.edu

European Journal of Physics

PAPER

A practical, quantitative electrostatics experiment

To cite this article: Bryan Armentrout and Diego Castaño 2019 *Eur. J. Phys.* **40** 035201

IOP Publishing European Journal of Physics
Eur. J. Phys. **40** (2019) 035201 (12pp) https://doi.org/10.1088/1361-6404/ab01b3

A practical, quantitative electrostatics experiment

Bryan Armentrout and Diego Castaño

Nova Southeastern University, United States of America

E-mail: castanod@nova.edu

Received 13 October 2018, revised 9 January 2019
Accepted for publication 24 January 2019
Published 26 February 2019

Abstract

An electrostatics experiment is presented that is practical, affordable, and quantitative. The equipment required is readily available and relatively inexpensive. The experiment relies on the electrostatic induction that results from a charged insulative plate in proximity to a conductive sphere. The experiment yields accesible results (a) under a variety of environmental conditions and results that (b) allow for quantitative analyses. These two characteristics distinguish it from most other simple electrostatics experiments. It is intended for college introductory physics students.

Keywords: electrostatics, method of images, Coulomb's law

1. Introduction

Experiments designed to demonstrate or test Coulomb's law typically involve some arrangement of conductors and/or insulators and exploit their electrostatic interaction. The simplest designs are altogether qualitative. All the designs intended to be quantitative are, not surprisingly, elaborate and costly. Among the quantitative designs, the prevailing one involves two conducting spheres and uses a torsion balance (following Coulomb's own method) to determine the electrostatic force between them. The cost of one experimental set-up of this type is close to three thousand dollars; a cost that is prohibitive for all without an ample budget. One of the difficulties concerns the establishment of a significant enough charge on the conducting spheres to result in a measurable force. To produce a force, say, minimally comparable to the weight of the spheres (assumed to be $\sim$0.10 N, for example, in the case of the spheres described below) requires a sphere charge on the order of tens of nanoCoulombs (assuming a centre-to-centre distance on the order of $\sim$0.10 m) [1]. The problem is that the typical sphere radius in these experiments is 0.02 m, and consequently the voltages required are in the kilovolt range. This requires either an alternating current kilovolt

power supply or a, perhaps more pedestrian, Wimshurst machine [2]. Such an arrangement presents prohibitive costs to many physics programs. In addition, the conducting spheres leak charge at a rate that is highly sensitive to atmospheric relative humidity.

Alternative arrangements using triboelectric charging prove to be more affordable; however, the initial charge produced proves to be lower than that provided by kilovolt power sources [3]. Since these setups are also highly sensitive to relative humidity, starting at a lower initial charge often proves unworkable in all but the driest environments.

In a high-humidity setting, we encountered significant difficulties designing a quantitative electrostatic experiment that yields data over manageable time intervals. Conducting pith balls discharge in a matter of seconds, even when charged with kilovolt devices. Employing an alternative approach, we worked with a combination of a single insulator, charged triboelectrically, which induced a dipole moment in an uncharged conducting sphere. This set-up offers two valuable advantages over those mentioned earlier: (1) materials are affordable and readily available; and (2) charge leakage, while still sensitive to relative humidity, occurs over the course of minutes instead of seconds. Our first trials involved a section of PVC tubing as an insulator. While the derivation of the theoretical electrostatic force was relatively straightforward, we noted that the measured maximum force was rather weak on our centigram mass scale. Our second trials employed a rectangular Teflon sheet, also charged triboelectrically. While the theoretical electrostatic force derivation was more complex for this arrangement, we noted a much greater maximum force, easily measured over the course of minutes on our mass scale, and robust under a range of relative humidity values. We believe this dual benefit of affordability and robustness under high humidity far outweighs any theoretical quantitative challenges inherent in the design.

In the following, we present a cost-effective experimental design intended for quantitative analyses of the electrostatic force and that does not require expensive kilovolt generating devices. In simplifying the experimental rig, we find that the form of the interaction law develops, what some students may find, distracting complications, especially in the dependence of the force on distance, to wit, the familiar point particle inverse square distance dependence is lost in the arrangement we propose. Nevertheless, the dependence of the force on the square of the charge is unchanged. To add to the ostensible disadvantages, the calculations involved in deriving the working formulas are beyond the scope of a typical class exposing students for the first time to electrostatics, however we believe excluding these theoretical details does not detract from the overall pedagogical benefits of the experiment. Despite these two drawbacks, the practicality of the design and its affordability more than makes up for the apparent shortcomings.

Sections 2 and 3 contain the main thrust of the paper. Therein we present the details of the set-up involved, propose the experimental procedure, and describe the analysis, making reference only to the working force equation and relegating its derivation to an appendix. Section 4 contains some of our results using the arrangement, and we make some concluding remarks in section 5. In appendix A, we calculate the force between a sphere and plate. In appendix B, we calculate the force between a sphere and pipe and discuss this version of the experiment. Both versions involve an *uncharged* conductive sphere similar to the ones discussed above.

2. The experimental set-up and procedure

The basic set-up involves an uncharged conductive sphere and an insulator, either a Teflon plate of dimensions $L \times W$ (figure 1) or a PVC pipe of length L (figure B1). The charging is

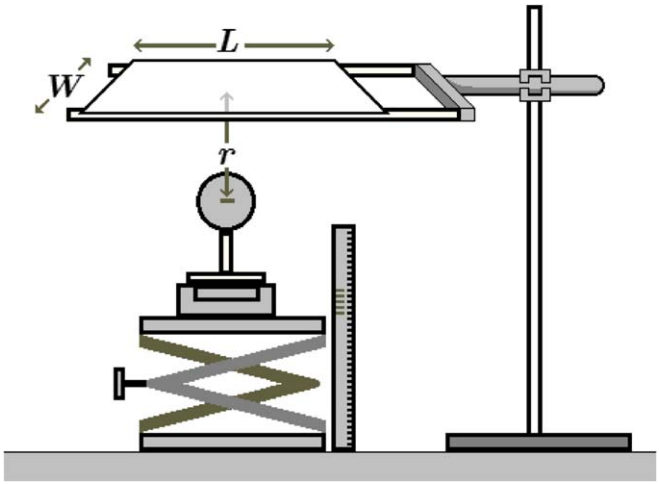

Figure 1. Sphere and plate set-up.

accomplished triboelectrically using a wool felt cloth on the insulator. We find that the Teflon charges better and maintains the charge longer than the PVC, having tested both under a range of atmospheric conditions usually encountered in the laboratory. We therefore recommend the Teflon plate for higher humidity conditions.

The materials needed consist of a Teflon sheet (10–15 cm on each side), wool felt cloth, a square balsa wood dowel, a balsa wood sheet, two hardwood dowels, conductive paint, a lab jack, a timer, a 0.01 g digital scale, and retort stand (with appropriate accessories such as universal clamp holder or Boss head, 3 prong extension clamp, double Burette clamp, etc). The sphere and base is constructed by gluing the balsa dowel and sheet to a ping-pong ball (whose typical radius is 2 cm). The ping-pong ball is then painted with conductive paint.

After arranging the various parts of the experiment along the lines of figure 1 (the sphere is directly under the plate, and its centre is equidistant from the four corners), the insulator is charged with the wool felt cloth. When the charged insulator is placed near the uncharged conducting sphere, the two will attract. The attractive force will result in a weight deficit, Δmg, for the sphere which is located on the scale calibrated to zero before the insulator is introduced. Students should be encouraged to qualitatively explore the charging process. This can be accomplished by charging the insulator to an assumed maximum value and temporarily setting it on the wooden dowels, noting the scale change (negative) value. We found that only a couple of rubs with the wool felt were sufficient to charge the Teflon plate to its maximum value. Further rubbing only served to discharge the plate and begin the charging process anew. Also, we noted that under conditions of low relative humidity and small separation, it is possible to establish a large enough initial charge on the plate that it will spontaneously discharge to the conductor when brought near it. If this occurs, a larger initial centre-to-centre separation value should be used.

Once the method of maximum charging has been established, we suggest setting the insulator on the wooden dowel(s), allowing the scale to reach its maximum (negative) value (this may take several seconds), and starting the timer when this value begins to decrease. Once a reading is taken at the first chosen elapsed time, the jack stand with conducting sphere should be slid out from under the insulator, to ensure the scale returns to zero. If it does not, it should be reset, and the stand should then be slid back under the insulator. This process

should be repeated in between each measurement. We found that leaving the conducting sphere arrangement underneath the insulator (specifically, the Teflon plate) throughout the measurements often results in a situation where the scale we employed does not return to a zero value when the jack stand arrangement is removed from under the insulator once the experiment is concluded. We suspect the effect is peculiar to the particular scales we employed, which seem to be susceptible to the electrostatic field. The procedure we have presented is intended to, and does, eliminate this possible problem.

For the case described in section 4 below, we chose to take readings at 10, 30, 50, 70, 90, 110, 130, and 150 seconds elapsed time at a fixed sphere-plate separation under conditions of comparatively low relative humidity (43%). The separation was then increased in increments of 1.0 cm. Finally, the entire process was repeated under conditions of higher relative humidity (58%).

3. Analysis

In the case of the Teflon plate, the working equation, i.e. the force between sphere and insulator, is valid for any sphere-plate separation distance

$$F = \frac{2k_e(\sigma A)^2R^3}{\lambda_p^5}f_A(r), \tag{1}$$

where σ is the plate's surface charge density (assumed uniform), R the radius of the sphere, f_A a dimensionless function of the sphere-plate separation distance, r in figure 1, and $\lambda_p = LW/2\sqrt{L^2 + W^2}$, a characteristic dimension for the plate. The function, f_A, can be ascertained from the results of appendix A. Note that this equation does not reflect the effects of the dielectric air on the interaction. The force equation has the form

$$F = Ck_eQ^2R^3f(r), \tag{2}$$

where Q is the charge of the insulator and C is a coefficient that depends on the dimensions of the insulator

$$C = \begin{cases} 2/\lambda_p^5, & \text{plate} \\ 4/L^5, & \text{pipe} \end{cases}. \tag{3}$$

The process of charging the insulator is haphazard. Therefore generating a precise charge is unfeasible and precisely reproducing a previously generated charge is also. One of the quantitative results of the experiment is the determination of the initial charge generated on the insulator. Once charged the insulator will lose its charge to an extent that depends significantly on the environmental humidity. This depletion will be described as an exponential decay

$$Q(t) = Q_0\mathrm{e}^{-\alpha t/2} \tag{4}$$

with

$$\tau = 2/\alpha \tag{5}$$

the e-folding time, and where Q_0 is the charge on the plate at $t = 0$. An experimental *run* is therefore characterised by the initial charge, Q_0. After charging and setting the insulator into place, data collection follows. Each data point in the run will consist of possibly three measurements: (a time, a distance, a mass scale reading). From the equations above, the relation among these variables and parameters can be expressed as follows (taking into

account that the attractive force registers a weight deficit, Δmg):

$$\frac{\Delta m}{m_s} = \frac{Ck_eQ_0^2R^3f(r)}{m_sg}\mathrm{e}^{-\alpha t}, \tag{6}$$

where m_s is the mass of the sphere and base. Taking the natural logarithm of this equation yields the relation

$$y \equiv \ln\left(\frac{m_s}{\Delta m}\right) = \alpha t + \beta \ln f(r) + \gamma, \tag{7}$$

where

$$\beta = -1 \tag{8}$$

$$\gamma = \ln\left[\frac{m_sg}{Ck_eQ_0^2R^3}\right] \tag{9}$$

which can be used as a linear regression equation to arrive at α and γ, for example, by fixing r. From γ, a determination of the initial charge load on the plate is possible, and $2/\alpha$ provides a characteristic time for the insulator's charge depletion given the environmental conditions in the laboratory during the experiment. Alternatively, r can be taken as the explanatory variable and regression can be used to determine γ and confirm β under very low humidity conditions for which $\alpha T \ll 1$, where T is the maximum elapsed time in the experimental run.

There is a limit that bears special consideration: the limit $r \gg \lambda_p$ (i.e. far from the plate). From the form of the function f_A (see appendix A), and to leading order

$$f_A(r) \approx (r/\lambda_p)^{-5}. \tag{10}$$

In this regime, we can rewrite equation (7):

$$y = \alpha t + \beta x + \gamma, \tag{11}$$

where $x = \ln(r/\lambda_p)$. In experimental runs consistent with these regimes, the data can then be used to perform a multi-linear regression, thereby establishing a best-fit plane (α, β, γ) in the three-dimensional space of variables, (t, x, y). Such experimentation can be used to confirm the exponent which the model predicts to be $\beta = -5$.

4. Some results

There are many procedures possible using the basic set-up described. Here we present some results for one such procedure that we had our students follow in the laboratory and that we therefore consider to be both simple and robust (largely insensitive to humidity). The aim of the experiment is the determination of the initial charge load, Q_0, on the Teflon plate after charging with a wool felt cloth. We fix the sphere-plate separation, r, in each experimental run and collect time and mass scale readings. The Teflon plate measured 15.0 cm on a side. The combined mass of the conducting sphere and attached balsa wood base was $m_s = 6.00$ g. The sphere's radius was $R = 2.0$ cm.

Table 1 shows scale change (absolute value) measurements at indicated times, with successive trials at increased sphere-plate separation. Although, for reasons outlined earlier, it is not possible to reliably establish a consistent initial charge, it can still be seen that sphere-plate separation and initial scale readings (and therefore force between insulator and conducting sphere) follow an inverse relationship. In addition, an exponential charge depletion pattern is noted for each trial. Interestingly, we noted larger depletion occurring earlier in the

Table 1. Low relative humidity (43%) series.

	Scale change, $\lvert\Delta m\rvert$ (g)				
Elapsed time, t (s)	$r = 3.0$ cm	$r = 4.0$ cm	$r = 5.0$ cm	$r = 6.0$ cm	$r = 7.0$ cm
10	2.20	1.65	1.05	0.73	0.61
30	2.00	1.48	1.05	0.71	0.58
50	1.89	1.37	0.98	0.69	0.57
70	1.78	1.30	0.91	0.64	0.52
90	1.64	1.23	0.79	0.64	0.50
110	1.59	1.16	0.75	0.60	0.48
130	1.52	1.12	0.72	0.56	0.42
150	1.45	1.07	0.67	0.55	0.42

Table 2. High relative humidity (58%) series.

	Scale change, $\lvert\Delta m\rvert$ (g)				
Elapsed time, t (s)	$r = 3.0$ cm	$r = 4.0$ cm	$r = 5.0$ cm	$r = 6.0$ cm	$r = 7.0$ cm
10	1.20	1.17	0.62	0.44	0.33
30	0.81	0.93	0.52	0.38	0.26
50	0.66	0.78	0.44	0.32	0.23
70	0.55	0.67	0.38	0.28	0.21
90	0.47	0.61	0.33	0.25	0.20
110	0.40	0.53	0.30	0.23	0.18
130	0.34	0.46	0.28	0.22	0.16
150	0.30	0.40	0.25	0.19	0.14

process (data not shown). There appears to be a complex charge saturation effect initially which takes about 10–20 s to subside. It results in a power law decay at first then transitions to an exponential decay. The procedure described in section 2 with respect to the timing of the first measurement is intended to circumvent this phenomenon.

We endeavoured to perform the experiment at the lowest and highest relative humidities reasonably expected given our geographical location. We achieved the low relative humidity of 43% by lowering the laboratory a/c temperature to 20 °C. We achieved a high relative humidity of 58% on an overcast day with the windows open.

Table 2 shows a repeat of the set of trials, this time in the higher relative humidity environment. Again, there is an inverse relationship in sphere-plate separation and initial scale reading. An exponential decay pattern is also present. However, some significant differences are apparent compared to table 1. It appears that the maximum initial possible charge is sensitive to relative humidity; namely, a higher relative humidity value results in a lower possible initial charge. In addition, the values established at 150 s elapsed time are much lower in a high relative humidity environment. Encouragingly, it can be seen that, even in this high relative humidity environment, useful data can still be taken across a wide variety of times and sphere-plate separations, proving the utility of this Coulomb-type experiment under a range of atmospheric conditions.

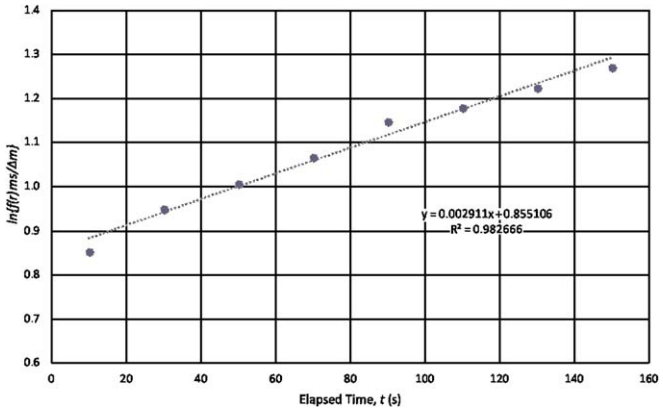

Figure 2. Typical regression analysis.

Table 3. Plate parameters for low relative humidity (43%) series.

	$r = 3.0$ cm	$r = 4.0$ cm	$r = 5.0$ cm	$r = 6.0$ cm	$r = 7.0$ cm
e-folding time, τ (s)	690	680	560	940	700
Initial charge, Q_0 (10^{-9} C)	770	760	740	710	770

Table 4. Plate parameters for high relative humidity (58%) series.

	$r = 3.0$ cm	$r = 4.0$ cm	$r = 5.0$ cm	$r = 6.0$ cm	$r = 7.0$ cm
e-folding time, τ (s)	210	270	310	350	370
Initial charge, Q_0 (10^{-9} C)	550	650	550	540	540

To aid in the quantitative determination of initial charge and e-folding time, we chose to provide our introductory college physics students an Excel spreadsheet, incorporating the pertinent equations, that allowed students to plot a linear regression to their data after simply entering sphere-plate separation, elapsed time, and scale (absolute value) readings. The slope of the linear regression leads to calculation of the e-folding time via equation (5). Likewise, the insulator's initial charge can be determined by the linear regression y-intercept value via

$$Q_0 = \left(\frac{m_s g \lambda_p^5}{2 k_e R^3 e^{\gamma}} \right)^{1/2}. \tag{12}$$

A typical fit with trial data is seen in figure 2.

The e-folding time and initial insulator charge for raw data in table 1 (low relative humidity) are found in table 3. The same results for raw data in table 2 (high relative humidity) are found in table 4.

Quantitative results support qualitative observations outlined previously. The amount of maximum initial charge is inversely related to relative humidity, and so is the e-folding time. It also appears that sphere-plate separation has little effect on the maximum possible amount of initial charge. This is to be expected, of course, since the charging process takes place in effective isolation of the sphere.

The results presented came from experimentation by the authors under the two extreme conditions described above. With time and practice, we refined our ability to prepare and execute the experiment to maximise the initial charge in each trial (i.e. by adjusting and then carefully replicating the charging process). For comparison, we present some student results. We collected the initial charge determination by a sample of eight student laboratory groups during various trials of the experiment this past Fall (all trials conducted under relative humidities of 52%–54%). The students typically only have a limited time to set up and perform the experiment which naturally often leads to poor execution and measurement. Moreover each experimental trial involved an unavoidably different charge initialisation which we have previously discussed, nevertheless one expects that the common conditions and similar equipment should result in comparable values for the initial charge, Q_0. In fact, for this sample we find $210\,\text{nC} \leqslant Q_0 \leqslant 560\,\text{nC}$ with a mean value of $350 \pm 20\,\text{nC}$. Considering the differences in the authors' versus the students' experimental conditions and techniques, the students' lower value for Q_0 compared to the authors' (see table 4) is not unexpected.

5. Conclusions

We presented an experimental design for a practical and cost-effective (quantitative) electrostatics experiment for introductory physics courses. We estimate that required materials should cost well under a hundred dollars which compares very favourably with commercially available Coulomb's law apparatus. The experimental design involves an uncharged conducting sphere and a charged insulator. We acknowledge one apparent drawback to be the more complex (than the point charge Coulomb case) form of the interaction force between the sphere and insulator and the advanced derivation of this force. Circumventing theoretical detours is not uncommon in introductory physics courses, so we believe this represents a minor glitch. The reliability and affordability of the design make the experiment a practical one for quantitative analyses of electrostatic interaction.

Appendix A. The force between an uncharged, conducting sphere and a finite, uniformly charged plane

The force between an uncharged, conducting sphere and a finite, uniformly charged plane is calculated. The method of images is used. Given a grounded conducting sphere and an external charged point particle, the interaction between the sphere and charged particle can be determined by considering a simpler arrangement involving two charged point particles, the original one and a second (image) particle within the space of the sphere. The charge of the image particle and its location are well-known functions of the sphere radius, the distance from the centre of the sphere to the external particle and its charge [4]. By considering the plane to be a continuous collection of point charges, we can use the solution to the sphere and charge problem just described and the calculus to solve the sphere and plane problem.

The sphere is centred at the origin. The uniform charged plane has dimensions, $L \times W$ ($\sigma = Q/LW$ is the assumed uniform surface charge density), is parallel to the xy-plane, and is centred on the z-axis at z_0 (see figure A1). Any charge $\mathrm{d}q$ on the plane has an image inside the sphere of charge

$$\mathrm{d}q' = -\frac{R}{r_p}\mathrm{d}q \tag{A1}$$

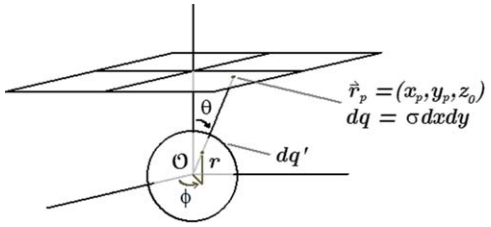

Figure A1. Conducting sphere and surface charge.

at a location along $\vec{r}_p$ (the location on the plane) a distance

$$r = \frac{R}{r_p} R \tag{A2}$$

from the origin, where

$$r_p^2 = x_p^2 + y_p^2 + z_0^2. \tag{A3}$$

This corresponds to a curved, non-uniform surface charge distribution. To ensure the sphere is uncharged, for each $\mathrm{d}q'$, there is a $-\mathrm{d}q'$ at the centre of the sphere. The force between the sphere and plane requires a (double) integral over the two charge distributions. However, a simpler approach is to calculate the dipole moment of the sphere due to the induced charge distribution

$$\vec{p} = \int \vec{r}' \, \mathrm{d}q'. \tag{A4}$$

Because the charge distribution is symmetrical across the x- and y-axes, $p_x = p_y = 0$, and only the z-component survives

$$p_z = \int r \cos\theta \, \mathrm{d}q', \tag{A5}$$

where $\cos\theta = z_0/r_p$, so

$$p_z = -\sigma R^3 z_0 \int \frac{\mathrm{d}x_p \mathrm{d}y_p}{r_p^3}. \tag{A6}$$

The force on this dipole is then given by

$$\vec{F} = (\vec{p} \cdot \nabla)\vec{E} \tag{A7}$$

$$= p_z \frac{\partial}{\partial z} \vec{E}. \tag{A8}$$

Only the z-component is relevant (and non-zero), so

$$F_z = p_z \frac{\partial E_z}{\partial z}\bigg|_{z=0}, \tag{A9}$$

where E_z is the electric field of the charged plane at the centre of the sphere. The dipole calculation yields

$$p_z = -\sigma R^3 z_0 \int_{-L/2}^{+L/2} \mathrm{d}x_p \int_{-W/2}^{+W/2} \mathrm{d}y_p (x_p^2 + y_p^2 + z_0^2)^{-3/2} \tag{A10}$$

$$= -4\sigma R^3 \sin^{-1}([1 + (z_0/\ell)^2]^{-1/2}[1 + (z_0/w)^2]^{-1/2}), \tag{A11}$$

where $\ell = L/2$ and $w = W/2$.

The electric field (due to the charged plane) at the centre of the sphere is calculated next. For this calculation, we locate the charged plane at $z = 0$, and determine its z-component of electric field at an arbitrary $z < 0$

$$E_z(z) = -4k_e\sigma \sin^{-1}([1 + (z/\ell)^2]^{-1/2}[1 + (z/w)^2]^{-1/2}). \tag{A12}$$

Note that

$$\lim_{\ell,w\to\infty} E_z(z) = -\frac{\sigma}{2\varepsilon_0}. \tag{A13}$$

From (A12), it follows that

$$\left.\frac{\mathrm{d}E_z}{\mathrm{d}z}\right|_{z=-z_0} = k_e\sigma A \frac{2z^2 + \ell^2 + w^2}{(z^2 + \ell^2)(z^2 + w^2)\sqrt{z^2 + \ell^2 + w^2}} \frac{z}{|z|}\Bigg|_{z=-z_0} \tag{A14}$$

$$= -k_e\sigma A \frac{2z_0^2 + \ell^2 + w^2}{(z_0^2 + \ell^2)(z_0^2 + w^2)\sqrt{z_0^2 + \ell^2 + w^2}}, \tag{A15}$$

where $A = LW$. We introduce the parameter $\eta = z_0/\lambda_p$, where

$$\frac{1}{\lambda_p^2} = \frac{1}{\ell^2} + \frac{1}{w^2} \tag{A16}$$

in terms of which the force has the final form

$$F = \frac{16k_e\sigma^2R^3}{\lambda_p} \frac{\left(1 + 32\frac{\lambda_p^4}{A^2}\eta^2\right)}{\left(1 + 16\frac{\lambda_p^4}{A^2}\eta^2\right)^{1/2}\left[1 + \eta^2 + 16\frac{\lambda_p^4}{A^2}\eta^4\right]} \sin^{-1}\left(\left[1 + \eta^2 + 16\frac{\lambda_p^4}{A^2}\eta^4\right]^{-1/2}\right) \tag{A17}$$

$$= \frac{2k_e\sigma^2A^2R^3}{\lambda_p^5} f_A(z_0), \tag{A18}$$

where

$$f_A(z_0) = \frac{8\lambda_p^4}{A^2} \frac{\left(1 + 32\frac{\lambda_p^4}{A^2}\eta^2\right)}{\left(1 + 16\frac{\lambda_p^4}{A^2}\eta^2\right)^{1/2}\left[1 + \eta^2 + 16\frac{\lambda_p^4}{A^2}\eta^4\right]} \sin^{-1}\left(\left[1 + \eta^2 + 16\frac{\lambda_p^4}{A^2}\eta^4\right]^{-1/2}\right). \tag{A19}$$

Appendix B. The force between an uncharged, conducting sphere and a finite, uniformly charged line

Here we present an alternate version of the experiment presented in section 2 involving a sphere and PVC pipe. We find the PVC pipe works well in low humidity conditions but fails to satisfactorily charge and hold the charge when relative humidity is 50% or greater. The

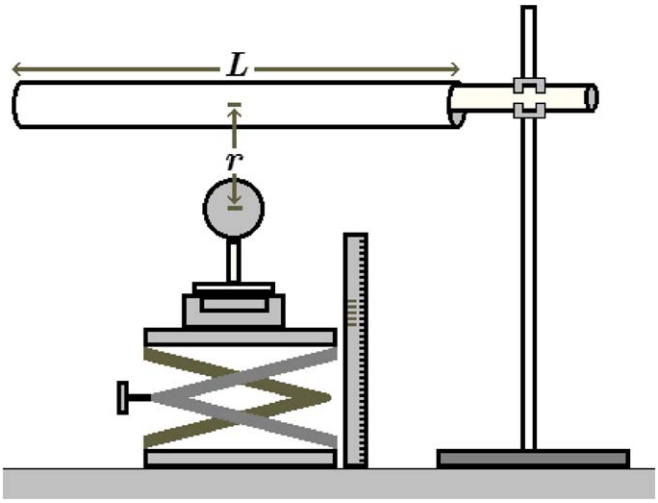

Figure B1. Sphere and pipe set-up.

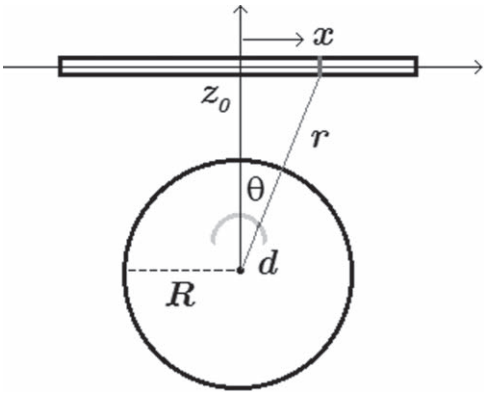

Figure B2. Conducting sphere and line charge.

arrangement is depicted in figure B1 (the sphere is directly under the pipe, and its centre is equidistant from the two ends).

The force between an uncharged, conducting sphere and a finite, uniform line charge is calculated using the method of images again and following the same idea described in appendix A. The sphere is centred at the origin. The uniform line charge of length, L (linear charge density $\lambda = Q/L$) is parallel to the x-axis and centred on the z-axis at z_0 (see figure B2). The electric field, E_z, of the line charge at the centre of the sphere is given by

$$E_z^{(\text{line})} = \frac{2k_e\lambda}{z_0}\frac{1}{[1 + (z_0/\ell)^2]^{1/2}}, \tag{B1}$$

where $\ell = L/2$. If we take the charge distribution to be (more accurately) uniformly spread on the surface of a tube, or pipe, of inside radius, $R_T \ll L$ (such that $\lambda = 2\pi R_T\sigma$), the field calculation leads to an elliptic integral, so we proceed approximately and expand accordingly

to arrive, in this case, at

$$E_z^{(\text{tube})} = \frac{2k_e\lambda}{z_0}\left\{1 - \frac{1}{2}\left[1 - 6\left(\frac{R_T}{L}\right)^2\right](z_0/\ell)^2 + \frac{3}{8}\left[1 - \frac{50}{3}\left(\frac{R_T}{L}\right)^2\right](z_0/\ell)^4 + \cdots\right\}. \quad \text{(B2)}$$

The force of attraction is then

$$F_z^{(\text{line})} = \frac{32k_e\lambda^2R^3}{L^3}\frac{1}{(z_0/\ell)^3}\frac{1 + 2(z_0/\ell)^2}{[1 + (z_0/\ell)^2]^2}, \quad \text{(B3)}$$

$$F_z^{(\text{tube})} = \frac{32k_e\lambda^2R^3}{L^3}\frac{1}{(z_0/\ell)^3}\left\{1 - 3\left(\frac{R_T}{L}\right)^2(z_0/\ell)^2 - \left[1 - \frac{81}{4}\left(\frac{R_T}{L}\right)^2\right](z_0/\ell)^4 + \cdots\right\}. \quad \text{(B4)}$$

We further express these as

$$F = \frac{4k_e(\lambda L)^2R^3}{L^5}f_B(z_0), \quad \text{(B5)}$$

where

$$f_B(z_0) = \begin{cases} \dfrac{8}{(z_0/\ell)^3}\dfrac{1 + 2(z_0/\ell)^2}{[1 + (z_0/\ell)^2]^2}, & \text{line} \\ \dfrac{8}{(z_0/\ell)^3}\left\{1 - 3\left(\dfrac{R_T}{L}\right)^2(z_0/\ell)^2 - \left[1 - \dfrac{81}{4}\left(\dfrac{R_T}{L}\right)^2\right](z_0/\ell)^4 + \cdots\right\}, & \text{pipe} \end{cases}. \quad \text{(B6)}$$

In the case of the pipe, note that in the limit in which $r \ll L/2$ (i.e. near the pipe), and to leading order, it follows that

$$f_B(r) \approx (r/L)^{-3}. \quad \text{(B7)}$$

As described in section 3 in the sphere and plate case, in this regime, a multi-linear regression can be used to establish the β parameter of equation (11) with $x = \ln(r/L)$, and confirm $\beta = -3$ in the pipe case.

ORCID iDs

Diego Castaño https://orcid.org/0000-0002-0308-8285

References

[1] Larson C O and Goss E W 1970 *Am. J. Phys.* **38** 1349
[2] Wiley P H and Stutzman W L 1978 *Am. J. Phys.* **46** 1131
[3] Cortel A 1999 *Phys. Teach.* **37** 447
[4] Griffiths D J 2013 *Introduction to Electrodynamics* 4 edn (Boston, MA: Pearson) p 127